RSC Advances

PAPER

View Article Online
View Journal | View Issue

Cite this: *RSC Adv.*, 2024, **14**, 14606

Photocatalytic degradation of methyl blue dye with H_2O_2 sensing†

Priyanka Sharma, Mainak Ganguly * and Mamta Sahu

Received 22nd February 2024
Accepted 26th April 2024

DOI: 10.1039/d4ra01354a

rsc.li/rsc-advances

A condensation polymer (urea-formaldehyde resin) passivated ZnO nanoparticles were used as an efficient photocatalyst for methyl blue degradation in the presence of H_2O_2 involving a Fenton-like reaction. The formation of $OH^{\bullet}$ radicals were attributed to the pivotal factor for the degradation process. The method was easy and recyclable. The dose of photocatalyst, initial dye concentration, pH variation, variations of the composition of the photocatalyst, and the effect of scavengers were gauged. The degraded product was highly fluorescent and fluorometric detection of H_2O_2 was achieved along with a colorimetric recognition pathway. No other dye could be degraded under similar experimental conditions, implying the novel utility of methyl blue for environmental remediation.

1 Introduction

Paper, plastics, leather, pharmaceuticals, food, cosmetics, dyestuffs, and textile dye effluents have always been a severe environmental hazard.[1] Several hues are poisonous and may have a direct impact on aquatic ecosystems.[2] Dyes are organic molecules with a complex aromatic molecular structure that may give other materials a vibrant and vivid color. However, dyes' complex aromatic molecular structures render them extremely persistent, making biodegradation more difficult. Methyl blue (MB) is a popular dye, that is used as a coloring agent and disinfectant in dyestuffs, rubbers, pharmaceuticals, insecticides, and varnish.[3]

Zinc oxide (ZnO) nanoparticles are inexpensive and easily manufactured on a big scale. ZnO is a heterogeneous n-type semiconductor with a large direct band gap of around 3.37 eV and an exciton binding energy of ~60 meV.[4] ZnO absorbs ultraviolet light (UV) at room temperature and responds poorly to visible light in the electromagnetic spectrum. This limits the intrinsic semiconductor's ability to function actively as a photocatalyst in the presence of a visible light source.[5]

Due to its potent oxidizing qualities, hydrogen peroxide (H_2O_2) has extensive applications in a range of chemical industries, food processing, environmental detection, and clinical treatment. H_2O_2 is also necessary for biological systems since it is a significant reactive oxygen species. For instance, human atherosclerosis, myocardial infection, and Alzheimer's disease have all been connected to unbalanced [H_2O_2]. According to a study, when [H_2O_2] levels are above 75 ppm, it is immediately harmful to human health.[6] In general, sensing H_2O_2 is critical in biological and chemical applications because it can serve as a versatile marker or messenger in interconnected chemical events. To identify H_2O_2, a range of techniques (such as spectrophotometry, chemiluminescence,[7] chromatography,[8] and colorimetric analysis) have been published. They are relatively complex, expensive, time-consuming, and prone to interference.[9] As a result, developing accurate, sensitive, easy, and quick detection of H_2O_2 is critical. Researchers have developed alternative techniques to satisfy comparable demands.

For the dye removal, two techniques were used. Adsorption is the purest and most friendly physical approach for the elimination of colors from contaminated aquatic bodies to save the lives of aquatic species and make the environment clean for human beings. A wide range of nanoparticles have been investigated for dye adsorption because of their high surface-to-volume ratio, which boosts adsorption capacity and efficiency, and the simplicity of altering surface functionality.[10–12]

Nanosized metal oxides, including MnO_2, Fe_2O_3, and ZnO, are hypothesized to have the ability to adsorb dyes from aqueous solutions.[10] With a large theoretical specific surface area, the actual application of ZnO in water cleaning, including decontamination and reuse, has received a lot of attention in recent years. ZnO has superior adsorption performance due to the presence of extra functional groups. Altıntığ *et al.*[11] utilized activated carbon loaded with zinc oxide nanoparticles as an eco-friendly adsorbent to remove malachite green from water efficiently. Zhang *et al.*[12] investigated the mechanism and adsorption of methyl blue on zinc oxide nanoparticles.

Adsorption is an effective method for removing colors, however, it cannot eliminate organic contaminants from contaminated aquatic systems. Because the effectiveness of

Department of Chemistry, Manipal University Jaipur, Jaipur-Ajmer Express Highway, Dehmi Kalan, Jaipur, Rajasthan 303007, India. E-mail: humansense2009@gmail.com

† Electronic supplementary information (ESI) available: Diagrammatic presentation of CP, digital images, *D*% with initial dye concentration & pH, TGA, XRD, EDS, recyclability, adsorption isotherm, scavengers study, LCMS, fluorescence data. See DOI: https://doi.org/10.1039/d4ra01354a

developed adsorption systems is insufficient, the photocatalytic degradation pathway is used to break down water-soluble organic dyes, making the environment safe for aquatic life and humans. This is comparatively a long and time-consuming process, but it is also very ecologically friendly and cost-effective. The extent of the nature of adsorption can be estimated using various adsorption isotherms (Langmuir, Freundlich, Elovich).[13,14]

One of the most popular advanced remediation techniques is photocatalytic degradation, which leaves a persistent trace when attempting to break the cycle by removing water from wastewater, breaking down human waste using light, or eliminating airborne pollutants. A redox mechanism known as photocatalytic degradation produces e^- and h^+ on the surfaces of nanoparticles. To promote photocatalysis, it is essential to select materials that can absorb light at all wavelengths. Water reacts with generated h^+ and e^- ions to produce radicals ($-O_2^{\bullet}$ and $-OH^{\bullet}$). The literature suggests that collecting impurities or states and generating crystal facets through microscopic surface design are essential for the greatest possible photocatalytic activity.

Venkatesan *et al.*[15] showed that ZnO nanoparticles were produced by utilizing leaf extract from *Solanum trilobatum*. The catalytic activity of produced ZnO NPs against the degradation of methylene blue dye was assessed together with optical, structural, and morphological features. The materials carbon dots (CDs), ZnO–N nanoparticles, and CD/ZnO–N nanocomposites were used as photocatalysts in the photodegradation of [methylene blue] (10 ppm) using a UV-B lamp 75 W for 60 minutes at ambient temperature. The effect of pH on methylene blue decolorization, as well as a cyclic test to determine the stability and reusable nature of the CD/ZnO–N photocatalyst.[16]

Metal oxide nanoparticles are widely valued because of their non-toxicity, chemical and physical stability, and biological properties, among other factors. ZnO, an II–VI semiconductor compound, is unique among metal oxide nanomaterials due to its peculiar properties and numerous applications. ZnO has a high exciton binding energy (60 meV), excellent optical gain at ambient temperature, and a high saturation velocity, among other properties. The optical properties of ZnO semiconductor materials are impacted by both internal and external causes. As electrons move between the conduction and valence bands, intrinsic effects arise. Extrinsic variables, such as dopant type and concentration, produce discrete electronic states that influence optical absorption.[17]

Polymer capping of nanoparticles offers several advantages in various applications, primarily due to the unique properties of polymers and their ability to tailor the surface chemistry and functionality of nanoparticles. Polymers contributed improved stability, controlled dispersion, surface functionalization, biocompatibility, tunable properties, multifunctionality, scalability, and cost-effectiveness to nanoparticles.[18]

There are reports available for polymer-capped nanoparticles. Guo *et al.*[19] used polyvinylpyrrolidone (PVP) as a capping polymer to stabilize ZnO nanoparticles. PVP surface treatment resulted in extremely monodisperse ZnO nanoparticles (3.760.3 nm) with increased UV luminescence and decreased visible luminescence. Tachikawa *et al.*[20] showed the optical properties of PVP-passivated ZnO nanoparticles. Sarkar *et al.*[21] reviewed the green polymeric nanomaterials for the degradation of dyes. Wang *et al.*[22] and Muzammal *et al.*[23] reviewed the polymer nanocomposite for photocatalytic degradation of azo dye.

Polymer is extensively used in modern research for the synthesis and protection of metal nanoparticles. We utilized CP, a condensation co-polymer of formaldehyde and urea[24] Fig. SI, ESI† for the synthesis of ZnO nanoparticles for the first time. Here, CP-capped ZnO nanoparticles were employed to eliminate toxic dye MB and sense H_2O_2 for environmental remediation. As ZnO is a well-known photocatalyst, we gauged its activity for the photocatalysis of MB dye. Moreover, we depicted the H_2O_2 sensing protocol as a corollary of photocatalysis. In the future, we would like to venture into other probable applications.

2 Experimental section

2.1 Materials and instruments

Without further purification, all the chemicals employed in the studies were of analytical grade. Triple-distilled water was used throughout the process. All glassware was cleaned with freshly prepared aqua regia, followed by soapy water and copious amounts of distilled water. Before use, the glassware was carefully dried. All metal salts, including zinc sulphate, urea, and formaldehyde, were obtained from Sigma Aldrich. Fisher Scientific and Qualigens supplied the NaOH, respectively. Fisher Scientific offered buffer tablets to calibrate the pH meter.

The Shimadzu UV-2600 digital spectrophotometer was used to collect all UV/Vis absorption spectra. The fluorescence was analyzed at room temperature using a Horiba FluoroMax-4 spectrometer. The JEOL Make JSM-7610FPlus FESEM, a high resolution (1 kV 1.0 nm, 15 kV 0.8 nm) scanning electron microscope with a wide range of probes, was used to investigate particle morphology. Samples were vacuum-dried for 24 hours before the FESEM experiment. Elemental analysis was performed using a JSM-7610F chamber equipped with an energy-dispersive X-ray spectrometer. For microscopic investigation, the water suspension was dried on carbon tape. pH solutions were produced using a Systronics Digital pH Meter 335. Liquid chromatography-mass spectra (LCMS) were recorded using a Xevo G2-S Q Tof mass spectrometer.

2.1.1 Synthesis of ZnO@CP. Urea (4 g) and zinc sulphate (0.161 g) were added in 10 mL of formaldehyde solution with shaking. Allowing the mixture to stand while stirring and add 2–3 drops of conc. HCl resulted in a white precipitate. After adding 20 mL of NaOH solution to it, the mixture was allowed to dry under sunlight. After drying, a white solid was obtained. The solid was crushed to make a white powder of ZnO@CP.

3 Results and discussion

3.1 Choice of MB

We disclosed MB dye for the sensing of H_2O_2 fluorometrically and colorimetrically. This paper also demonstrated the

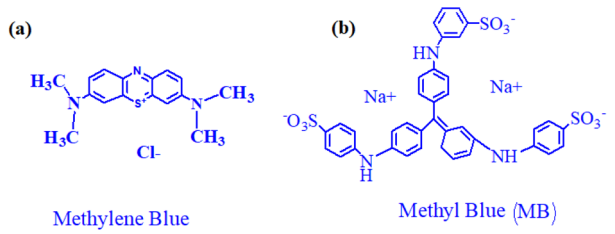

Fig. 1 Structure of methylene blue and methyl blue (MB) dyes.

degradation of toxic MB dye *via* a fast cost-effective, recyclable, energetically favorable, and biocompatible pathway. Simultaneous detection and remediation of toxic materials are reported for the first time, the main essence of the paper. There are few reports available on the nanoparticle-based degradation of MB.[25–34] Polymer-capped nanoparticles for MB elimination are not available in the literature.

Though there are reports available for methylene blue degradation,[35–51] there is no report in the literature for MB degradation in the presence of H_2O_2. Moreover, the origin of fluorescent species after the treatment of H_2O_2 and photocatalyst with dye for sensing applications is completely novel, as reported in this manuscript.

Since methylene blue is one of the most often used industrial dyes, it is frequently utilized in literature to evaluate the effectiveness of recently developed adsorbent materials. By employing hydrogels' swelling, adsorption, and water-holding capacities, methylene blue can be successfully removed from wastewater.[49] [Fig. 1(a)].

Commonly used dye MB ($C_{37}H_{27}N_3Na_2O_9S_3$) is poisonous and nonbiodegradable. When released into the environment, it severely damages aquatic ecosystems by raising the chemical and biological oxygen demand of water bodies, decreasing light penetration, and interfering with photosynthesis.[25] [Fig. 1(b)]. Table 1 summarizes the removal of MB in the presence of nanoparticles with physico-chemical conditions.

The degradation of MB has only a few reports. No report is available for MB dye degradation employing H_2O_2. The present work is associated with a report of degradation, along with fluorometric and colorimetric sensing applications. We investigated with other dyes (methylene blue, methyl red, and methyl orange) employing a similar protocol (ZnO@CP/H_2O_2/sunlight). Fig. S2, ESI† denoted that removal of these dyes was not possible under similar experimental conditions. Thus, MB was very selective in our experimental conditions.

Many other toxic dyes (Congo red, methyl orange) are released from the industries,[52,53] Pesticides,[54] fungicides,[55] novel dyes[56] and discharged pharma ingredients,[57] are also toxic and a threat to the environment. We will study the degradation of such toxic pollutants also in the future.

3.2 Photodegradation of MB with ZnO@CP in the presence of H_2O_2

Zinc oxide-impregnated CP (ZnO@CP) was added in blue-colored MB (MBZnO@CP) solution under sunlight for 30 min. No significant change was observed in the solution. However, the introduction of H_2O_2 to Zn-impregnated CP and 30 min sunlight treatment made the solution colorless (ZnO@CPH). We also varied other metal ions (Ag^+, Pb^{2+}, Na^+, K^+, Cd^{2+}, Co^{3+}, Cr^{2+}, Ni^{2+}, Ba^{2+}, Mg^{2+}, Ca^{2+}) *in lieu* of Zn^{2+} and repeated the synthetic procedure of metal impregnated CP. Interestingly, no metal ion could make the MB solution colorless, unlike Zn^{2+} under similar experimental conditions. Decolorization by ZnO@CPH was not affected by pH change. Such observation concluded that ZnO@CPH under sunlight exposure caused photochemical degradation of MB and it was an irreversible process. Fig. 2, depicted A_a/A_c (A_a = absorbance in the presence of different metal-impregnated CP + MB + H_2O_2; A_c = MB + H_2O_2). We exposed MB with ZnO@CPH at different time domains on a certain day. We found that between 11.30 am to 12.30 pm, the flux density was highest and photodegradation was faster (Fig. 3). We varied the exposure time and found that 30 min exposure could break MB (10^{-2} M) quantitively at that

Table 1 Nanoparticles-based removal of MB dyes with various physico-chemical aspects

Nanoparticles	Size/morphology	Removal technique adsorption/degradation	Rate constant (min^{-1})	Condition of removal	Apparatus to monitor
Zinc oxide (Guo *et al.*)[19]	25 ± 5 nm	Adsorption	—	Room temperature	UV-Vis spectrometer
Iron oxide[26]	12 nm/spherical	Adsorption	—	Room temperature	UV-Vis spectrometer
Fe_3O_4/SiO_2 (Ali *et al.*)[27]	25 ± 5 nm	Adsorption	—	Room temperature	UV-Vis spectrometer
$MgFe_2O_4$ (Liu *et al.*)[28]	50 nm/polycrystalline	Adsorption	—	Room temperature	UV-Vis spectrometer
Fe_3O_4 (Fana *et al.*)[29]	100 nm/spherical	Adsorption	—	30 °C	UV-Vis spectrometer
$MnFe_2O_4$ (Zhang *et al.*)[30]	86–94 nm	Adsorption	—	298 K	UV-Vis spectrometer
$Mn_{0.5}Co_{0.5}Fe_2O_4$ (Liu *et al.*)[31]	25 nm/crystalline	Adsorption	—	Room temperature	UV-Vis spectrometer
Fe $(NO_3)_3 \cdot 9H_2O$ (Azama *et al.*)[32]	—	Adsorption	—	Room temperature	UV-Vis spectrometer
Co_3O_4 (Dhiman *et al.*)[33]	47 nm/spherical	Degradation	0.023		Solar
$ZnFe_2O_4$ (Li *et al.*)[34]	18 nm/polycrystalline	Adsorption	—	Room temperature	UV-Vis spectrometer
ZnO (present study)	~800 nm/spherical	Degradation	1×10^{-1}	Sunlight	UV-Vis spectrometer/fluorometric

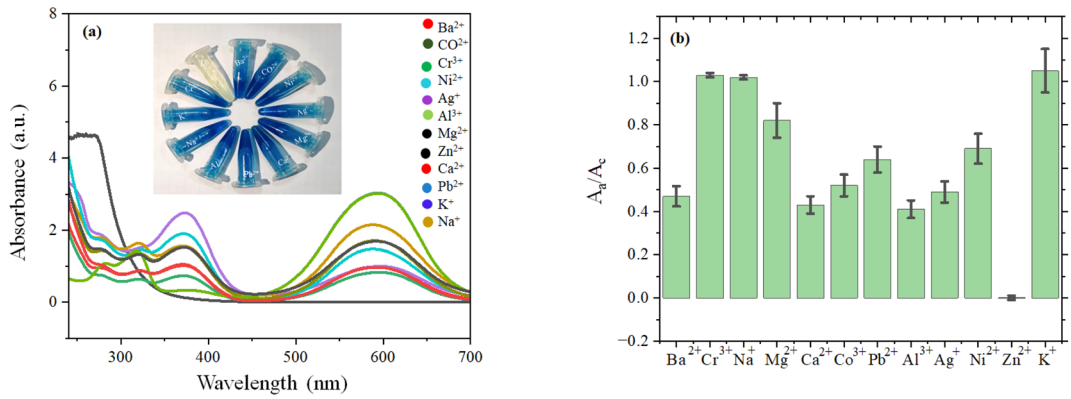

Fig. 2 (a) UV-Vis spectra and digital image and (b) bar diagram of absorbance variation of different metals impregnated CP with MB dye (under 30 min sunlight exposure).

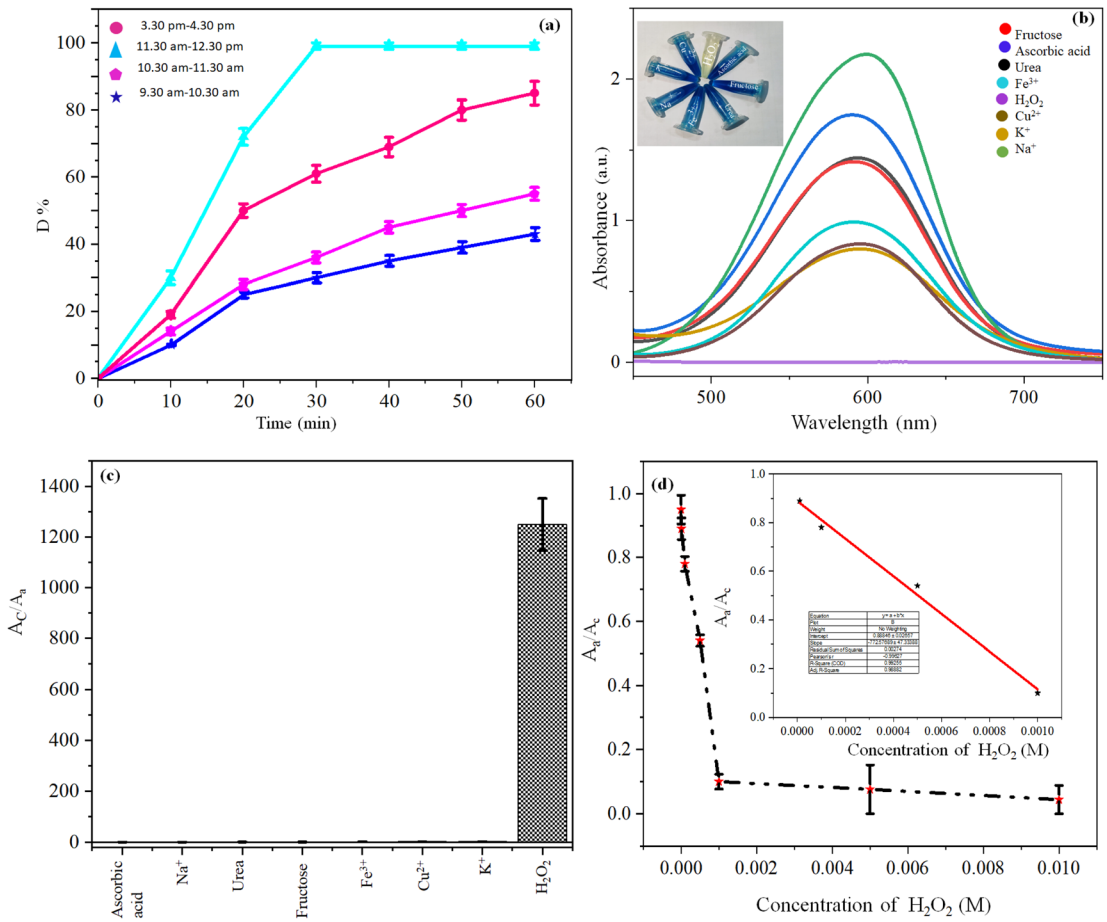

Fig. 3 (a) Influence of sunlight exposure on MB removal with ZnO@CP at various time domains of a certain day; (b) UV-Vis spectra and digital image and (c) bar diagram of ZnO@CP with H_2O_2 & other competing molecules; (d) change of absorbance with [H_2O_2] and LOD of H_2O_2 detection.

time domain. Thus, flux was directly proportional to the rate of degradation.

3.3 Colorimetric sensing of H_2O_2

To understand the role of H_2O_2 we introduced fructose, ascorbic acid, urea, K^+, Fe^{3+}, Cu^{2+}, and Na^+ (competing molecules[58] of H_2O_2) to ZnO@CP instead of H_2O_2. Such competitive reagents could not decolor MB, justifying the selectivity of the H_2O_2 sensor. As depicted in Fig. 3 A_a/A_c (A_a = absorbance of MBZnO@CP in the presence of analytes at 597 nm; A_c = absorbance of MBZnO@CP in the absence of analytes at 597 nm) was much lower for H_2O_2 (0.0008) than fructose (0.69),

ascorbic acid (0.86), urea (0.71), K^+ (0.42), Fe^{3+}(0.48), Cu^{2+}(0.39), Na^+ (1.07). Naked eyes could detect H_2O_2 contamination in water up to 5×10^{-5} M by tallying with blue coloration. However, a linear detection range was observed from 0.005 M to 10^{-5} M with a limit of detection (LOD) 10^{-5} M.

3.4 Kinetics of MB photodegradation

Degradation (D%) (eqn (1)) at time t with various doses of ZnO@CP in the presence of H_2O_2 (10^{-2} M) are shown following the following equation (under the Sun). C_0 and C_t are the MB concentrations at time 0 and t respectively.

$$D\% = \frac{C_0 - C_t}{C_0} \times 100 \quad (1)$$

$$\ln\frac{C_0}{C_t} = kt \quad (2)$$

Table 2 indicates that increased [ZnO@CP] up to 1.5 g dm^{-3} enhanced the MB removal efficiency [Fig. 4]. Exceeding 1.5 g dm^{-3} resulted in an unfavorable effect of photodegradation owing to the aggregation of ZnO@CP, which made the surface inaccessible for photon absorption. Furthermore, the turbidity of the solution reduced UV light penetration, lowering photodegradation efficiency. The photocatalytic process was found to be pseudo-first order. The slope of the fitting line corresponds to the value of the rate constant k (min^{-1}) (eqn (2)).

ZnO@CP was synthesized at various molar ratio of CP and ZnO for the degradation study (Table 3). The highest degradation efficiency was observed at [Urea] : [formaldehyde] : [ZnO] = [66] : [133] : [1].

We varied the initial concentrations (0.05 M, 10^{-2} M, 5×10^{-3} M, 10^{-3} M, 5×10^{-4} M, 10^{-4} M) of MB dye in Fig. S3, ESI.† With the decrease of the dye concentration, D% was increased. Such an inverse relation was attributed to the rise of internal optical density, making the solution impermeable to sunlight.[59] On the other hand, the degradation was effective in neutral and alkaline pH. Highest D% was observed at pH 12. Probably at acidic pH $OH^{\bullet}$ radicals were quenched, causing a decrease in D%.

Table 2 D% and rate constant of MB photodegradation with variable ZnO@CP doses and H_2O_2

Doses (g dm^{-3})	0	0.5	1	1.5	2
D%	0	65	75	99	85
k (min^{-1})	—	3×10^{-2}	4×10^{-2}	1×10^{-1}	7×10^{-2}

3.5 Significance of sunlight exposure

Sunlight exposure (30 min) was vital for the synthesis of ZnO@CP to degrade MB with H_2O_2. 200 W bulb exposure (from 9 cm above), dark and heat (100 °C) during the synthesis of ZnO@CP caused D% 0.8%, 97%, and 98% respectively (Scheme 1).

3.6 Characterization of ZnO@CP

Thermogravimetric analysis (TGA) (Fig. S4, ESI†) was used to investigate the thermal profile of ZnO@CP at a 10 °C min^{-1}

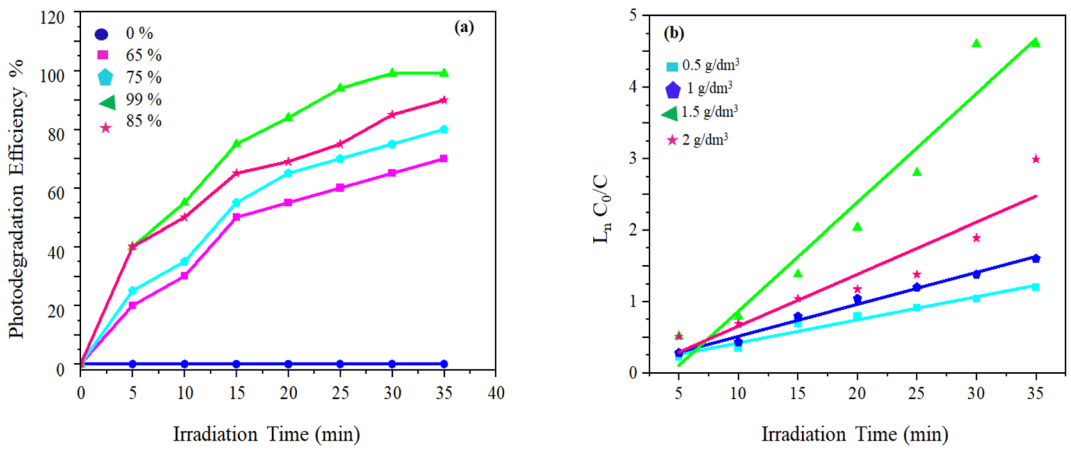

Fig. 4 (a) Influence of the amount of ZnO@CP and (b) linear simulation kinetics curves for photocatalytic degradation of MB under the sun.

Table 3 Rate constant of MB photodegradation with 1.5 g dm^{-3} ZnO@CP (various [urea] : [formaldehyde] : [ZnO]) and H_2O_2

Precursor of polymer (CP)		Moles of zinc acetate	Amount of ZnO@CP applied	[Urea] : [formaldehyde] : [ZnO]	k (min^{-1})
Moles of urea	Moles of formaldehyde				
0.066	0.133	0.001	1.5 g dm^{-3}	66 : 133 : 1	1.0×10^{-1}
0.066	0.133	0.05	1.5 g dm^{-3}	1.32 : 2.66 : 1	4.1×10^{-2}
0.066	0.133	0.0005	1.5 g dm^{-3}	132 : 266 : 1	2.3×10^{-2}

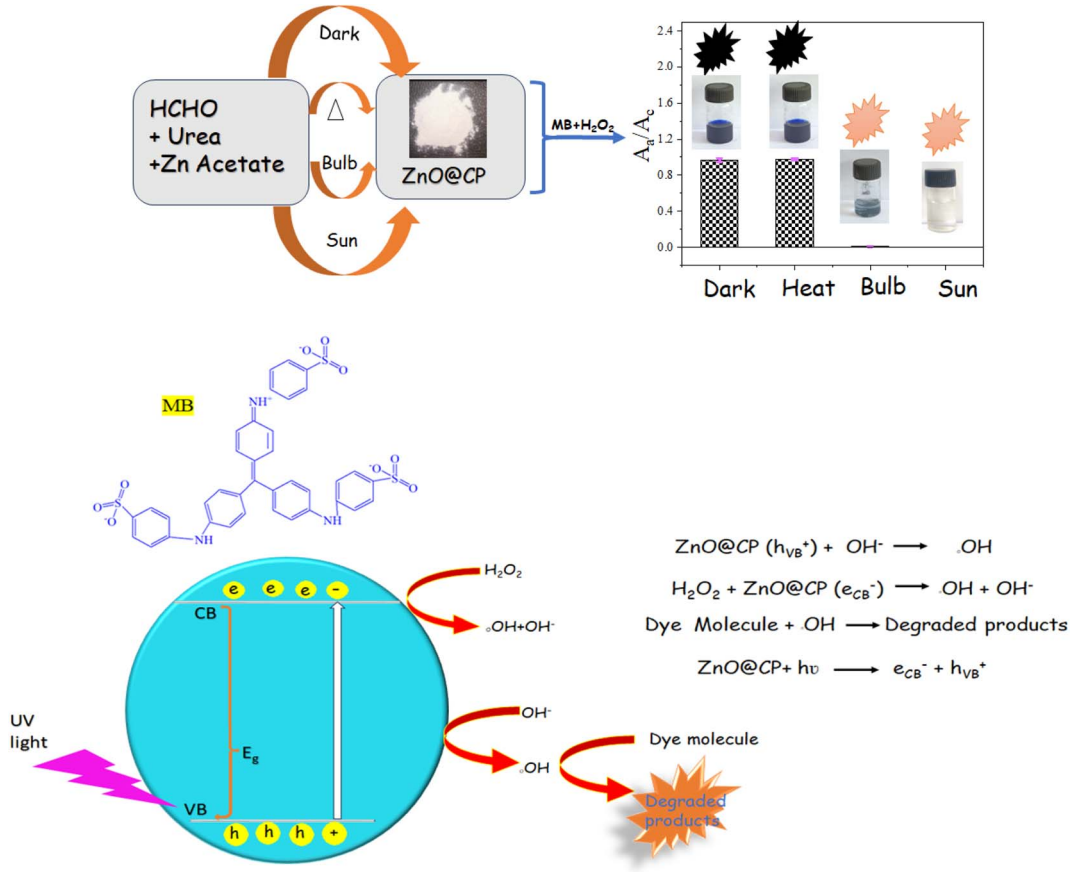

Scheme 1 Synthesis of ZnO@CP and mechanism of degradation for MB with H_2O_2 sensing.

heating rate in the air within the 800 °C temperature range. Initially, a weight loss of 12.9% and 20.42% for CP and ZnO@CP respectively was observed in the thermogram attributed to the desorption of physiosorbed water. Moreover, a steep weight loss, as well as cramped weight loss of 63.8% and 23.3%, was due to the thermal degradation of covalently bonded organic scaffolds of CP. On the contrary, the high residual weight (13.55%) was attributed to the production of thermostable ZnO in ZnO@CP, and no crap was obtained, demonstrating the nanoparticle's stability.[60] Such type of polymerization was associated with different polymer molecules (with different degrees of polymerization).[61] Polymers with a low degree of polymerization decomposed in the temperature range of 200 °C to 500 °C, associated with 87.1% weight loss. On the other hand, polymer passivated ZnO (ZnO@CP) had a comparatively higher degree of polymerization. Thus, 66.03% weight loss happened in between temperatures 200 °C to 370 °C. After that, no further weight loss was observed. The residual mass was due to ZnO and long-chain polymers.

Powder XRD analyses confirmed the formation of ZnO in ZnO@CP. According to the XRD analysis, the XRD peak of the CP was very intense and broad (2θ 10°–35°), as denoted by the black trace (Fig. S5, ESI†). So, the peak of ZnO was not shown clearly. One new peak with a 2θ value of 31.75° represented the (100) plane for ZnO in ZnO@CP (blue trace). It is noteworthy that the intense peak intensity of the polymer implied the increased crystallite nature and decreased amorphous nature.[62] No other peak of ZnO was observable in XRD spectra due to the efficient coating of polymer over ZnO (Fig. 5).

The formation of ZnO in ZnO@CP was further confirmed with XPS analysis. The peak with a binding energy of 1021.8 eV corresponded to Zn $2p_{3/2}$, when Zn was in the form of ZnO.[63] However, the other XPS peak of Zn $2p_{1/2}$ at 1043.8 eV was 2 eV towards higher binding energy indicating strong capping of CP on ZnO. From the FESEM images, it was evident that ZnO@CP showed porous micro-flowers (~800 nm) with sharp-tipped nano petals (~10 nm). The elemental analysis of the corresponding to the FESEM image confirmed the presence of Zn at the surface (Fig. S6, ESI†). Low-resolution images indicated that micro-flowers were spherical and a bit aggregated. The spherical shape of ZnO particles with CP capping (with a sort of aggregation) was also confirmed by TEM images, where each particle was of ~800 nm diameter. The crystalline nature was also confirmed *via* the arranged pattern of bright dots from the SAED (Selected area electron diffraction) image (Fig. 5).

3.7 Recyclability of ZnO@CP

After treating 1.5 g dm^{-3} of ZnO@CP in 50 mL 10^{-2} M MB with 10^{-2} M H_2O_2 under 30 min sunlight exposure D% was calculated for the first cycle (by monitoring the difference in

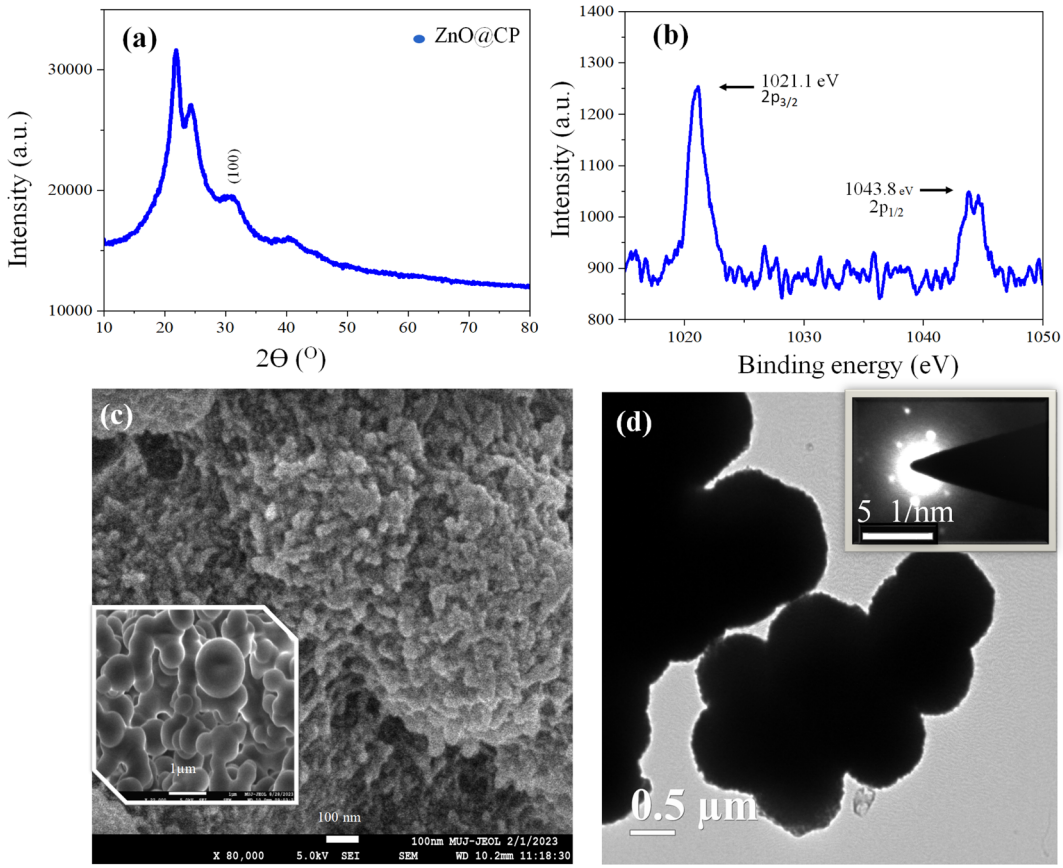

Fig. 5 (a) XRD, (b) XPS, (c) FESEM (high resolution, low resolution, and (d) TEM & SAED of ZnO@CP.

absorbance with and without catalyst). The ZnO@CP was filtered out, washed with water, dried, and added in 50 mL 10^{-2} M MB with 10^{-2} M H_2O_2 under 30 min sunlight exposure to calculate the *D*% for the second cycle. Similarly, *D*% was calculated for 3rd, 4th, and 5th cycles. For the first cycle, second cycle, third cycle, fourth cycle, and fifth cycle, the % of removal was 99%, 94%, 85%, 79%, and 72% respectively. The decrease in removal efficiency with the increased number of cycles might be due to an irreversible change in surface morphology (Fig. S7, ESI†).

3.8 Mechanism of dye removal

For the first time, we reported MB degradation with polymer-capped ZnO and H_2O_2. It is noteworthy that ZnO@CP could adsorb MB efficiently in a monolayer fashion. Attempting to fit in Langmuir, Elovich, and Frudnlich isotherms we found that the adsorption of MB was Langmuir type (maximum uptake capacity Q_m = 100.4 mg dm^{-3}) (Fig. S8, ESI†). However, the introduction of H_2O_2 switched the process to photodegradation. Excitation of the e^- from the valence band (VB) to the conduction band (CB) happened during UV light irradiation, resulting in the formation of the e^- and h^+ in the CB &VB, respectively. The e^-, transferred in the CB combined with H_2O_2 molecules to generate oxidative species OH˙ radicals, while photoinduced holes left in the VB accept electrons from the hydroxyl group, generating highly oxidative OH˙ radicals that were responsible for the degradation of MB dye molecules (Scheme 1). Addition of radical scavenger ascorbic acid, EDTA ([Scavenger]/[H_2O_2] = 1, molar ratio) substantially decreased *D*%, implying the significance of OH˙ radicals for degradation. The degradation efficiency was 59% suppressed when EDTA was employed and 62% suppressed when ascorbic acid and 41% suppressed when IPA was added at the same volume and concentration. EDTA and ascorbic acid as serve as a h^+ scavenger, while IPA is used as an OH˙ scavenger.[64–66] Thus, h^+ and ˙OH are necessary for photocatalysis, with ˙OH having a bigger impact than h^+ [Fig. S9, ESI†].

The OH˙ radical formation in the presence of ZnO and H_2O_2 was supported by various literature and mass spectra analysis (Fig. S10, ESI†). Ali *et al.*[67] demonstrated the photodegradation of methylene blue dye using UV/H_2O_2. Naikwade *et al.*[68] demonstrated the photocatalytic degradation of methyl orange using a magnetically retrievable supported ionic liquid phase photocatalyst using H_2O_2.

The treatment of ZnO@CPH with MB under the light of 30 min followed by filtration resulted in a colorless solution with strong fluorescence measured by a fluorimeter. We varied the excitation wavelength from 260 nm to 420 nm and found that maximum fluorescence intensity was observed at an excitation wavelength of 360 nm.

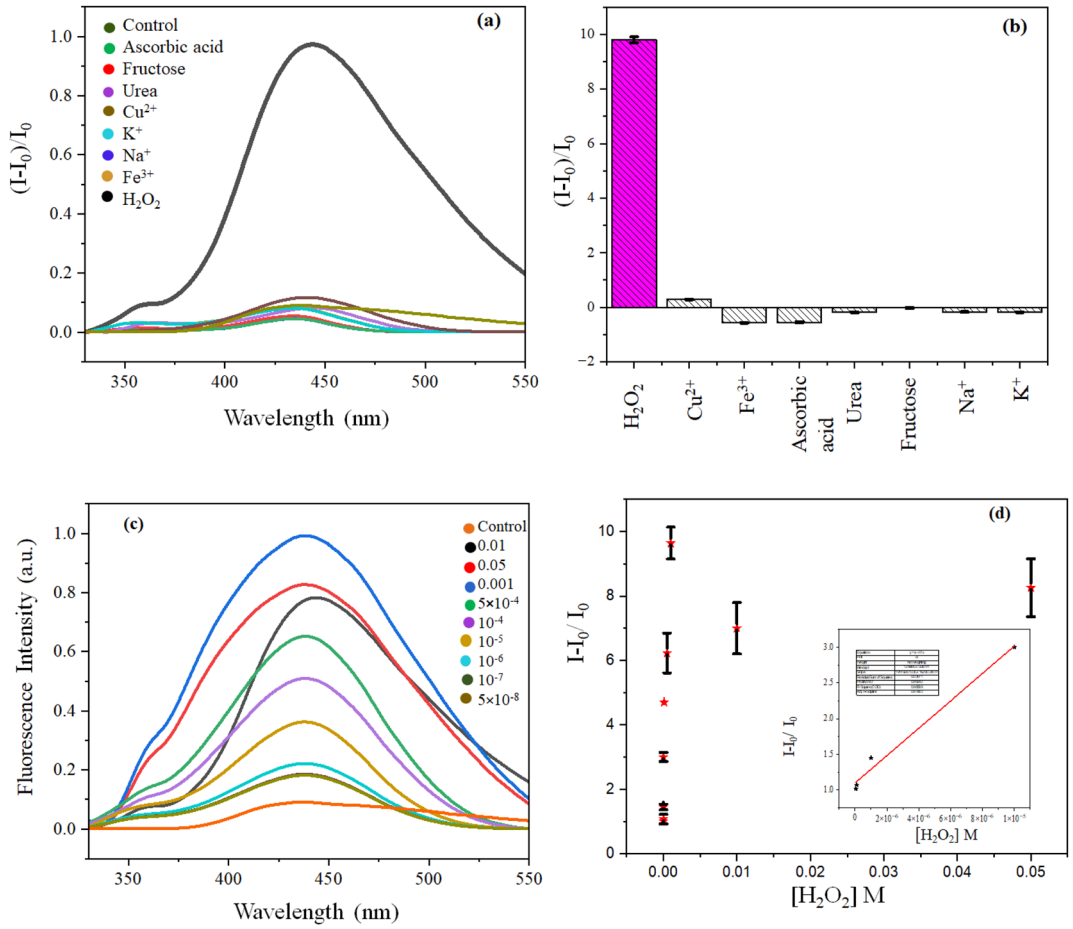

Fig. 6 (a) Fluorescence spectra and (b) bar diagram of ZnO@CP with H_2O_2 & other competing molecules; (c) fluorescence spectra with [H_2O_2] and (d) LOD of H_2O_2 detection.

We obtained a very small fragment of 99.00 (SO_2+ H_2O+ $OH^{\bullet}$) (from LCMS), which was the main (dominant) fragment, justifying the process of degradation. Moreover, Fig. S10, ESI† indicated the cleavage of the C–N bond with the formation of X and Y (the structures of fragments were depicted in Fig. S10, ESI†). X and/or Y might be decent fluorophores to generate high emissions of MB dye after ZnO@CP/H_2O_2/sunlight treatment. Further research is warranted in the future to understand the nature of the *in situ*-generated fluorophore at various physico-chemical conditions.

3.9 Fluorometric sensing of H_2O_2

Though we were able to sense H_2O_2 selectively calorimetrically, the LOD was 10^{-5} M only. To further increase the LOD we employed fluorescence spectroscopy. After the treatment of ZnO@CPH with MB under the light of 30 min, a colorless solution was obtained with highly emissive behaviour (λ_{em} 437 nm and λ_{ex} 360 nm). In other words, the degraded products of MB were fluorescent. Such behavior prompted us to design a fluorometric H_2O_2 sensor. With the increase of [H_2O_2], the fluorescence was increased due to the formation of increased $OH^{\bullet}$ radicals, capable of degrading MB. Thus, an increase in H_2O_2 concentrations caused the increase in the concentration of degraded MB with the gradual enhancement of fluorescence. So increased [H_2O_2] associated with increasing fluorescence was helpful for H_2O_2 sensing (Fig. 6).

Though the fluorescence was decreased monotonously up to the concentration of 5×10^{-8} M, a linear detection range was observed between 10^{-5} M to 5×10^{-8} M with a limit of detection 5×10^{-8} M and linear regression (R^2) 0.985. No competing material (K^+, Na^+, ascorbic acid, urea, fructose, Cu^{2+}, Fe^{3+}) could exhibit such evolution of fluorescence, unlike H_2O_2, as they could not degrade MB, unlike H_2O_2. We also studied the effect of interfering materials in the colorless degraded solution of MB during the sensing of H_2O_2. No other coexisted interfering agent could alter the originated fluorescence of degraded MB except Fe^{3+} (Fig. 6 and S11, ESI†).

4 Conclusions

This work showed that toxic dye MB could be photodegraded effectively in the presence of sunlight by employing H_2O_2. The rate of degradation decreased significantly in the presence of $OH^{\bullet}$ the radical scavenger. These $OH^{\bullet}$ radicals proceeded through an oxidation process that produces intermediates, $OH^{\bullet}$, CO_2, SO_2, and H_2O at the end. However, after the

photodegradation a strong fluorophore was generated, accelerating the sensitive and selective sensing platform. Future research is warranted to investigate the origin of fluorescence after MB degradation. The proposed tactic can be used for the remediation of other toxic materials like pesticides, fungicides, waste pharma materials, novel dyes, *etc.* We believe that the present paper may be highly helpful for young researchers venturing into the field of circular economy.

Conflicts of interest

There are no conflicts to declare.

Acknowledgements

The authors are thankful to CAF & SAIF (MUJ) for the instrumental facility.

Notes and references

1 (*a*) M. Anbia and S. Salehi, *Dyes Pigm.*, 2012, **1**, 1–9; (*b*) G. Z. Kyzas, M. Kostoglou, A. Vassiliou and N. K. Lazaridis, *Chem. Eng. J.*, 2011, **2**, 577–585; (*c*) S. C. Hsieh and P. Y. Lin, *J. Nanopart. Res.*, 2012, **14**, 956.

2 (*a*) J. Ma, Y. Jia, Y. Jing, Y. Yao and J. Sun, *Dyes Pigm.*, 2012, **3**, 1441–1446; (*b*) R. Cheng, S. Ou, B. Xiang, Y. Li and Q. Liao, *Langmuir*, 2009, **2**, 752–758; (*c*) A. C. Lucilha, C. E. Bonancea, W. J. Barreto and K. Takashima, *Spectrochim. Acta, Part A*, 2010, **75**, 389–393; (*d*) Z. X. Chen, Y. Cheng, Z. L. Chen, M. Megharaj and R. Naidu, *J. Nanopart. Res.*, 2012, **8**, 899–915.

3 (*a*) Y. Wang and J. Yu, *Water Res.*, 1999, **33**, 3512; (*b*) T. Wu, X. Cai, S. Tan, H. Li, J. Liu and W. Yang, *Chem. Eng. J.*, 2011, **1**, 144–149.

4 (*a*) C. C. Chen, P. Liu and C. H. Lu, *Chem. Eng. J.*, 2008, **3**, 509–513; (*b*) X. Wang, Y. Ding, C. J. Summers and Z. L. Wang, *J. Phys. Chem. B*, 2004, **26**, 8773–8777; (*c*) Z. L. Wang and J. Song, *Science*, 2006, **312**, 242–246; (*d*) A. Janotti and C. G. Van de Walle, *Rep. Prog. Phys.*, 2009, **12**, 126501; (*e*) Y. Zhang, M. K. Ram, E. K. Stefanakos and D. Y. Goswami, *J. Nanomater.*, 2012, **2012**, 1–22.

5 (*a*) J. Wellings, N. Chaure, S. Heavens and I. Dharmadasa, *Thin Solid Films*, 2008, **12**, 3893–3898; (*b*) M. Nirmala, M. G. Nair, K. Rekha, A. Anukaliani, S. Samdarshi and R. G. Nair, *Afr. J. Basic Appl. Sci.*, 2010, **2**, 161–166; (*c*) I. S. J. Bao, Z. Su, R. Gurwitz, F. Capasso, X. Wang and Z. Ren, *Nanoscale Res. Lett.*, 2011, **404**, 1–7.

6 (*a*) J. Sun, C. Li, Y. Qi, S. Guo and X. Liang, *Sensors*, 2016, **16**, 584; (*b*) G. He, F. Gao, W. Li, P. Li, X. Zhang, H. Yin, B. Yang, Y. Liu and S. Zhang, *Anal. Methods*, 2019, **11**, 1651–1656; (*c*) H. Wei and E. Wang, *Anal. Chem.*, 2008, **80**, 2250–2254; (*d*) M. Hoshino, S. Kamino, M. Doi, S. Takada, S. Mitani, R. Yanagihara, M. Asano, T. Yamaguchi and Y. Fujita, *Spectrochim. Acta, Part A*, 2014, **117**, 814–816.

7 (*a*) Y. Huiyun, W. Haijun, X. Chengyi, C. Yaqin and Y. Ruo, *Biosens. Bioelectron.*, 2018, **116**, 16–22; (*b*) X. Jiang, H. Wang, R. Yuan and Y. Chai, *Anal. Chem.*, 2018, **90**, 8462–8469; (*c*) H. Yue, X. Bu, M.-H. Huang, J. Young and T. Raglione, *Int. J. Pharm.*, 2009, **375**, 33–40.

8 (*a*) P. Gimeno, C. Bousquet, N. Lassu, A.-F. Maggio, C. Civade, C. Brenier and L. Lempereur, *J. Pharm. Biomed. Anal.*, 2015, **107**, 386–393; (*b*) Q. Liu, P. Chen, Z. Xu, M. Chen, Y. Ding, K. Yue and J. Xu, *Sens. Actuators, B*, 2017, **251**, 339–348; (*c*) P. J. Rivero, E. Ibanez, J. Goicoechea, A. Urrutia, I. R. Matias and F. Arregui, *Sens. Actuators, B*, 2017, **251**, 624–631.

9 (*a*) G. Jiaojiao, L. Hui, P. Lingyan, G. Kai and L. Junqi, *ACS Appl. Mater. Interfaces*, 2018, **10**, 30441–30450; (*b*) Z. Ya, Z. Zhifeng, W. Fangfang, T. Jing, P. Tao, L. Bingqing, W. Honggui and Y. Shixue, *Sens. Actuators, B*, 2018, **275**, 155–162.

10 W. S. Al-Arjan, *Polymers*, 2022, **15**, 3086.

11 E. Altıntıg, M. Yenigun, A. Sarı, H. Altundag, M. Tuzen and T. A. Saleh, *Environ. Technol. Innovation*, 2021, **21**, 101305.

12 F. Zhang, J. Lan, Y. Yang and T. Wei, *J. Nanopart. Res.*, 2013, **15**, 2034.

13 V. Batra, I. Kaur and D. Pathania, Sonu, *Appl. Surf. Sci. Adv.*, 2022, **11**, 100314.

14 M. Ganguly and P. A. Ariya, *ACS Omega*, 2019, **7**, 12107–112120.

15 S. Venkatesan, S. Suresh, P. Ramu, J. Arumugam, S. Thambidurai and N. Pugazhenthiran, *Results Chem.*, 2022, **4**, 100637.

16 D. G. Ayu, S. Gea, N. Andriayani, D. J. Telaumbanua, A. F. R. Piliang, M. Harahap, Z. Yen, R. Goei and A. I. Y. Tok, *ACS Omega*, 2023, **17**, 14965–14984.

17 R. Kumar, G. Kumar and A. Umar, *Nanosci. Nanotechnol. Lett.*, 2014, **8**, 631–650.

18 X. Zhang, Y. Zhao, H. Zhang, W. Chen, S. Guo and Y. Chen, *Org. Biomol. Chem.*, 2016, **14**, 4815–4830.

19 L. Guo, S. Yang, C. Yang, P. Yu, J. Wang, W. Ge and G. K. L. Wong, *Appl. Phys. Lett.*, 2000, **76**, 2901–2903.

20 S. Tachikawa, A. Noguchi, T. Tsuge, M. Hara, O. Odawara and H. Wada, *Materials*, 2011, 1132–1143.

21 S. Sarkar, N. T. Ponce, A. Banerjee, R. Bandopadhyay, S. Rajendran and E. Lichtfouse, *Environ. Chem. Lett.*, 2020, **18**, 1569–1580.

22 E. Z. Wang, Y. Wang and D. Xiao, *Polymers*, 2021, **8**, 1215.

23 S. Muzammal, A. Ahmad, M. Sheraz, J. Kim, S. Ali, M. B. Hanif, I. Hussain, S. Pandiaraj, A. Alodhayb, M. S. Javed, H. A. Z. Al-bonsrulah and M. Motola, *Energy Convers. Manage.: X*, 2024, **22**, 100547.

24 (*a*) S. Kumar, N. Dilbaghi, R. Rani and G. Bhanjana, *J. Bionanosci.*, 2012, **4**, 227–250; (*b*) Y.-Q. Liu, Y. Tian, G.-Z. Zhao, Y.-Y. Sun, F.-T. Zhu and Y. Cao, *J. Polym. Res.*, 2008, **15**, 501–505.

25 F. Zhang, J. Lan, Y. Yang, T. Wei, R. Tan and W. Song, *J. Nanopart. Res.*, 2013, **15**, 2034.

26 N. J. Singh, B. Wareppam, S. Ghosh, B. P. Sahu, P. K. AjiKumar, H. P. Singh, S. Chakraborty, S. S. Pati, A. C. Oliveira, S. Barg, V. K. Garg and L. H. Singh, *Nanotechnology*, 2020, **31**, 425703.

27 N. S. M. Ali, H. A. Alalwan, A. H. Alminshid and M. M. Mohammed, *Pollution*, 2022, **8**, 295–302.

28 R. Liu, P. Lv, H. Fu, R. Lu, X. Wu and Y. Lu, *J. Nanosci. Nanotechnol.*, 2017, **17**, 4755–4762.
29 L. Fana, Y. Zhang, C. Luoa, F. Lua, H. Qiua and M. Suna, *Int. J. Biol. Macromol.*, 2012, **50**, 444–450.
30 L. Zhang, Y. Zhang, L. Yang, X. Jiang and Q. Yang, *Desalin. Water Treat.*, 2014, 1–11.
31 Y. Liu, Q. Yu, X. Liu and R. Liu, *Environ. Prog. Sustainable Energy*, 2019, **38**, S277–S287.
32 K. Azama, R. Razab, N. Shezada, M. Shabira, W. Yang, N. Ahmada, I. Shafiqa, P. Akhterd, A. Razzaqa and M. Hussaina, *J. Environ. Chem. Eng.*, 2020, **5**, 104220.
33 S. Dhiman and B. Gupta, *Environ. Technol. Innovation*, 2021, **23**, 101765.
34 S. Li, Q. Liu, R. Liu, R. Lu and J. Xiang, *J. Nanosci. Nanotechnol.*, 2017, **17**, 4112–4118.
35 M. A. Abu-Dalo, S. A. Al-Rosan and B. A. Albiss, *Polymers*, 2021, **19**, 3451.
36 S. Venkatesan, S. Suresh, P. Ramu, J. Arumugam, S. Thambidurai and N. Pugazhenthiran, *Results Chem.*, 2022, **4**, 100637.
37 A. Bhapkar, R. Prasad, D. Jaspal, M. Shirolkar, Kh. Gheisari and S. Bhame, *Inorg. Chem. Commun.*, 2023, **148**, 110311.
38 G. Ankamwar, K. Balaprasad, B. Vaishali, I. Annsi, Jose, Sarma, S. Loka, Mahajan and M. Chandrashekhar, *J. Nanosci. Nanotechnol.*, 2017, **17**, 1185–1192.
39 D. G. Ayu, S. Gea, Andriayani, D. J. Telaumbanua, A. F. R. Piliang, M. Harahap, Z. Yen, R. Goei and A. I. Y. Tok, *ACS Omega*, 2023, **17**, 14965–14984.
40 K. A. Isai and V. S. Shrivastava, *SN Appl. Sci.*, 2019, **1**, 1247.
41 A. Negash, S. Mohammed, H. D. Weldekirstos, A. D. Ambaye and M. Gashu, *Sci. Rep.*, 2023, **13**, 22234.
42 A. Balcha, O. P. Yadav and T. Dey, *Environ. Sci. Pollut. Res. Int.*, 2016, **24**, 25485–25493.
43 P. B. Koli, K. H. Kapadnis, U. G. Deshpande and M. R. Patil, *J. Nanostruct. Chem.*, 2018, **8**, 453–463.
44 P. B. Koli, K. H. Kapadnis and U. G. Deshpande, *J. Environ. Eng.*, 2019, **7**, 103373.
45 R. S. Shinde, S. D. Khairnar, M. R. Patil, V. A. Adole, P. B. Koli, V. V. Deshmane, D. K. Halwar, R. A. Shinde, T. B. Pawar, B. S. Jagdale and A. V. Patil, *J. Inorg. Organomet. Polym.*, 2022, **32**, 1045–1066.
46 R. H. Waghchaure, V. A. Adole, B. S. Jagdale and P. B. Koli, *Inorg. Chem. Commun.*, 2022, **140**, 109450.
47 S. A. Ahire, A. A. Bachhav, T. B. Pawar, B. S. Jagdale, A. V. Patil and P. B. Koli, *Results Chem.*, 2022, **4**, 100633.
48 P. B. Koli, S. G. Shinde, K. H. Kapadnis, A. P. Patil, M. P. Shinde, S. D. Khairnar, D. B. Sonawane and R. S. Ingale, *J. Indian Chem. Soc.*, 2021, **98**, 100225.
49 S. A. Ahire, A. A. Bachhav, B. S. Jagdale, A. Patil, P. B. Koli and T. Pawar, *J. Inorg. Organomet. Polym. Mater.*, 2023, **33**, 1–12.
50 R. H. Waghchaure, P. B. Koli, V. A. Adole and B. S. Jagdale, *Results Chem.*, 2022, **4**, 100488.
51 M. A. Ali, I. M. Maafa and I. Y. Qudsieh, *Water*, 2024, **16**, 453.
52 J. Gaur, K. Vikrant, K.-H. Kim, S. Kumar, M. Pal, R. Badru, S. Masand and J. Momoh, *Mater. Today Sustain.*, 2023, **22**, 100339.
53 J. Kaur, S. Bansal and S. Singhal, *Phys. B*, 2013, **416**, 33–38.
54 S. H. Khan and B. Pathak, *Environ. Nanotechnol. Monit. Manag.*, 2020, **13**, 100290.
55 P. Purkait, A. Bhattacharyya, S. Roy, S. Maitra, G. C. Das and M. G. Chaudhuri, *Int. J. Environ. Anal. Chem.*, 2023, **103**, 307–325.
56 M. Chijioke-Okere, N. J. Okorocha, B. N. Anukam and E. Emanuel Oguzie, *Int. Lett. Chem., Phys. Astron.*, 2019, **81**, 18–26.
57 R. Mohammed, M. E. M. Ali, E. Gomma and M. Mohsen, *J. Environ. Chem. Eng.*, 2020, **5**, 104295.
58 P. Sharma and M. Ganguly, *New J. Chem.*, 2023, **47**, 7481–7485.
59 J.-C. Sin, S.-M. Lam, A. R. Mohamed and K.-T. Lee, *Int. J. Photoenergy*, 2012, **2012**, 1–23.
60 A. G. Naikwade, M. B. Jagadale, D. P. Kale, A. D. Gophane, K. M. Garadkar and G. S. Rashinkar, *ACS Omega*, 2020, **5**, 131–144.
61 A. Sánchez-Ferrer, D. Rogez and P. Martinoty, *RSC Adv.*, 2015, **5**, 6758–6770.
62 (*a*) A. K. Zak, R. Razali, H. A. W. Majid and M. Darroudi, *Int. J. Nanomed.*, 2011, **6**, 1399–1403; (*b*) S. A. Bhat, F. Zafar, A. U. Mirza, A. H. Mondal, A. Kareem, Q. M. R. Haq and N. Nishat, *Arab. J. Chem.*, 2020, **13**, 5724–5739.
63 (*a*) X. Liu, H. L. Liu, W. X. Zhang, X. M. Li, N. Fang, X. H. Wang and J. Wu, *Nanoscale Res. Lett.*, 2015, **10**, 1–9; (*b*) A. Kruth, S. Hasen, T. Beweries and V. Bruser, *ChemSusChem*, 2013, **1**, 152–159.
64 Y. Zhu, J. Xue, T. Xu, G. He and H. Chen, *J. Mater. Sci.: Mater. Electron.*, 2017, **28**, 8519.
65 L. Ye, J. Liu, C. Gong, L. Tian, T. Peng and L. Zan, *ACS Catal.*, 2012, **2**, 1677.
66 B.-J. Yang, W. Luo, Q. Liao, J.-Y. Zhu, M. Gan, X.-D. Liu and G.-Z. Qiu, *Trans. Nonferrous Met. Soc. China*, 2020, **30**, 200–211.
67 M. A. Ali, I. M. Maafa and I. Y. Qudsieh, *Water*, 2024, **16**, 453.
68 A. G. Naikwad, M. B. Jagadale, D. P. Kale, A. D. Gophane, K. M. Garadkar and G. S. Rashinkar, *ACS Omega*, 2020, **5**, 131–144.